Vanadate Conformation Variations in Novel Vanadium Pentoxide Nanostructures

C. O'Dwyer,[†] V. Lavayen,[†,‡] S. B. Newcomb,[∥] M. A. Santa Ana,[‡] E. Benavente,[§]

G. González,[‡] and C. M. Sotomayor Torres[†]

[†] *Tyndall National Institute, University College Cork, Cork, Ireland*

[‡] *Department of Chemistry, Faculty of Science,*

Universidad de Chile, Santiago, Chile

[∥] *Glebe Scientific Limited, Newport, Co. Tipperary, Ireland and*

[§] *Department of Chemistry, Universidad Tecnológica Metropolitana, Santiago, Chile*

Abstract

We report the comparative structural-vibrational study of novel nanostructures of nano-urchin, nanotubes and nanorods of vanadium oxide. The tube walls comprise layers of vanadium oxide with the organic surfactant intercalated between atomic layers. Both Raman scattering and infrared spectroscopies showed that the structure of nano-urchin, nanotubes and nanorods of vanadium oxide nanocomposite are strongly dependent on the valency of the vanadium, its associated interactions with the organic surfactant template and the packing mechanism and arrangement of the surfactant between vanadate layers. Accurate assignment of the vibrational modes to the V−O co-ordinations has allowed their comparative classification and relation to atomic layer structure. Although all structures are formed from the same precursor, differences in vanadate conformations due to the hydrothermal treatment and surfactant type result in variable degrees of crystalline order in the final nanostructure. The nanotube-containing nano-urchin contain vanadate layers in the nanotubes that are in a distorted $\gamma-V^{5+}$ conformation, whereas the the nanorods, by comparison, show evidence for V^{5+} and V^{4+} species-containing ordered VOx lamina.

I. INTRODUCTION

One-dimensional nanomaterials, such as nanotubes [1, 2], nanowires [3], and nanobelts or nanoribbons [4–6] have attracted considerable attention in the past decade because of their novel and useful physical properties leading to numerous potential applications. Although the majority of research and development has been based on carbon nanotubes, considerable attention is now being directed to transition metal nanostructures based on their metal oxides which, due to their versatile chemical properties often modulable by changes in the oxidation state of in the metal coordination sphere, may lead to a variety of products and tunable materials [7, 8].

Some vanadium oxide-based low dimensional products have been studied extensively [9–11]. Starting from the laminar V_2O_5 xerogel [8] numerous two dimensional organic-inorganic intercalation products have been obtained [12]. Many of these V_2O_5 based nanostructures may be obtained in quantities of the order of grams [13]. The possibility of synthesizing new varieties of shapes and sizes can only be possible by a better understanding of the molecular conformation of these very ordered structures and will encourage their potential application in new kinds of optical, electrical and charge storage architectures.

Hydrothermal treatment of either of these laminar composites, especially those intercalated with long-chained amines or directly from the precursors, results in one dimensional tubular products with practical quantitative yields [14, 15]. Together with the electrical and morphological properties of vanadium oxide derivatives, this has encouraged its study as a potential new functional material, and applications such as optical switches [16], gas sensoring [17] and as electrodes in lithium rechargeable batteries [18] have been reported. The efficiency reached in the preparation of laminar and tubular nanostructures is necessary

but not solely sufficient for integration of these materials in devices; specimens formed by ordered and dense arrays of uniform nanostructures are desired, hence the recent successful realization of the nano-urchin [13]. All structures are, however, heavily reliant on the vanadate conformation after hydrothermal treatment and the organic template used for their ultimate morphology and properties.

In this work, we present a comparative structural-vibrational study of nano-urchin and nanorods of vanadium oxide recently reported by our group [13–15] and compare and contrast the observations with earlier attempts by others with vanadate-based low-dimensional products. Both Raman scattering and infrared spectroscopies highlight variations in the crystal order of the vanadate atomic layers, depending on the synthesis conditions and the V^{4+}/V^{5+} ratio in the nanostructures.

II. EXPERIMENTAL

A. Synthesis of Vanadium Oxide (VOx) Nanostructures

The method employed for the synthesis of vanadium pentoxide nanotubes and nano-urchin were previously described in Refs [12, 13, 15]. Vanadium pentoxide nanorods were obtained from an aqueous solution of NH_4VO_3 mixed with octa-, hexa-, or do-decylamine (ODA, HDA, DDA: containing 18, 16 and 12 C atoms in each alkyl chain respectively) in a molar ratio of 2:1. After vigorous stirring, where all the inorganic compound was completely dissolved, the *p*H of the solution was adjusted with a solution of HCl. The resultant yellow suspension was constantly stirred for 48 h. The hydrothermal treatment (HT) of the yellow suspension was performed in a Teflon lined autoclave at 453 K for several days. The product was washed several times with ethanol and with doubly deionized pure

water and subsequently dried under vacuum (10^{-3} mm Hg) for 48 h at room temperature.

B. Methods of Characterization

X-ray powder diffraction characterization was performed using a SIEMENS D5000 diffractometer (Cu-K_α, $\lambda = 0.15418$ nm, operation voltage 40 kV, current 30 mA). The morphological characterization of the nanostructured products was performed by field emission scanning electron microscopy (FESEM) using a JEOL JSM-6700F FESEM operating at beam voltages between 1-10 kV. Electron transparent specimens were prepared by ion-milling techniques and placed on a holey carbon support. Transmission electron microscopy (TEM) and selected area electron diffraction (SAED) were conducted using a Philips CM300 FEGTEM operating at 300 kV. The chemical composition of the samples was determined by elemental chemical analysis using a SISONS model EA-1108 analyzer. The Fourier transform infrared (FTIR) spectra were recorded using a KBr pellet technique on a Perkin-Elmer series 2000 apparatus in the region $4000-450$ cm^{-1}. Raman spectroscopy was conducted using a Jobin Yvon XY 800 spectrometer equipped with a cooled charge coupled device (CCD) detector. Samples of both the nano-urchin and the nanorods were filtered through highly ordered porous alumina templates to prevent any laminar pieces of the bulk nanocomposite from adding to the spectral contribution of the nanostructures. The spectral excitation was provided by an argon ion laser, using a 514.5 nm laser line (2.41 eV) with a variable laser power density.

III. RESULTS AND DISCUSSION

Figure 1a shows an FESEM micrograph of a cluster of spherical vanadium oxide nano-urchin. Each nano-urchin contains a relatively high volume of nanotubes with a volumetric density of $\sim$40 sr^{-1} [13]. The tubes are approximately 9$-$12 μm in length with overall outer diameters of 100$-$200 nm; a typical FESEM image of the nanotubes as can be seen in the inset to Fig. 1a. The vanadium oxide nanorods, on the other hand, have a length of typically $\sim$1 μm, and a diameter in the range of 100$-$200 nm [15]. A typical FESEM image of a group of nanorods can be seen in Fig. 1b.

HRTEM data, shown in Fig. 2, was acquired for nanotubes at an advanced stage of their formation. It can be observed that the sidewall regions are characterized by the 2.85 nm spacing of the lattice fringes, determined by SAED measurements (inset) and the tubes are composed of orthorhombic V_2O_5 layers. The central core of the nanotube is observed to be hollow and extends to the very tip. The inner hollow core is straight and maintains a constant diameter surrounded by an equal number of alternating contrast lines resulting from diffraction from similarly spaced vanadate atomic layers and we have determined that the organic surfactant used during synthesis of the nanostructure is in an *all-trans* configuration between these ordered and parallel successive layers [14]. Overall, the tube is structurally uniform and from diffraction contrast in these images, the scrolling of the vanadate layers is apparent. The uniformity in atomic layers renders the vanadium oxide nanostructures amenable to quantitative structural analysis through spectroscopic measurements.

The X-ray diffraction (XRD) analysis of the products after hydrothermal treatment (HT), shown in Fig. 3a, shows that the reaction leads to specific crystalline products; the $\{00l\}$ Bragg reflections indicate a lamellar intercalated product of the amine and the vanadium

oxide. The (001) reflection has the highest intensity and is located at a d value of 2.9 nm corroborating the SAED measurements. The characteristic $\{hk0\}$ reflections, shown in Fig. 3b, indexed on the basis of a two-dimensional square lattice with $a = 0.611$ nm, indicate high structural order of both the vanadate layers but also for the intercalated amine groups between these layers, *i.e.* these peaks appear at the same 2Θ values even when we employed longer or shorter chained amines as the structural template. The degree of crystallinity is impressive considering that during data acquisition, the nanotubes are oriented in a radial array in the case of the nano-urchin structure, and without any predefined preferential respective orientation in the case of the nanorods. The amine chain length did proportionately affect the intensity of the $\{00l\}$ peaks, however. Thus, the hydrothermal treatment of the reaction mixture leads to the formation of a crystalline mesophase formed by lamellar species with interlaminar distances of ∼3 nm. Both the XRD and SAED results were confirmed by elemental chemical analysis, where the final HDA-containing nanorods, for example, have the composition $V_2O_5(HDA)_{0.83}{\cdot}1.8H_2O$. Analysis [exp. (calculated for $C_{13.28}H_{32.65}N_{0.83}O_{6.8}V_2$)]: C: 39.06 (38.32); H: 8.05 (7.89); N: 2.56 (2.79). The composition of this mesophase agrees with the intercalation rate expected for a double layer of amine intercalated between the inorganic walls of the nanostructures which are in turn formed by a double layer of VO_4 tetrahedrons [19].

A. Raman Scattering Spectroscopy of Vanadium Pentoxide Xerogel, Nanotubes and Nanorods

The Raman scattering spectrum of the xerogel is presented in Fig. 4a. During acquisition, the V_2O_5 xerogel was targeted with laser radiation with a power density of 1312 μW μm^{-2}. After the measurements, no sample damage was observed.

The xerogel is known to exhibit a bilayered structure along the c-axis of the monoclinic unit cell [20]. The monoclinic unit cell typically shows a lower symmetry compared with the bulk V_2O_5 [21] resulting in the Raman modes of the $V_2O_5{\cdot}0.6H_2O$ xerogel being observed at 291, 308, 416, 703, 881, 966, 974, and 1001 cm^{-1} as seen in Fig. 4a. Of these, the peaks corresponding to the phonon modes of the V=O bending vibration are observed at 291 and 416 cm^{-1}. The higher frequency modes originating from stretching vibrational modes of V−O groups (ν_{V-O}) are observed at 308 and 703 cm^{-1}. Stretching vibrational modes of the vanadyl group (V=O) are observed at 966, 974, and 1001 cm^{-1}, in agreement with the values reported in Ref. [21].

Figure 4b shows the Raman scattering spectra for the nanotubes in the nano-urchin, formed by hydrothermal treatment of the ODA surfactant-containing xerogel as outlined in Section II.A. The vibrational spectroscopic observations of the nano-urchin were acquired over extended time periods at much lower laser power densities (291 μW μm^{-2}) as slight damage was observed in the nanostructures at power densities greater than 436 μW μm^{-2}.

The uniquely structured nano-urchin of vanadium pentoxide exhibit a vibrational mode at 504 cm^{-1} that is assigned to the triply coordinated oxygen (V_3−0) by comparison with previous reports [22]. The spectral peak in Fig. 4b observed at 643 cm^{-1} is assigned to the doubly coordinated oxygen (V_2−O) stretching mode that results from edge-shared oxygen atoms in common with three pyramidal vanadyl unit cells [23]. This vibration is not typically observed in free-standing vanadium oxide nanotubes and is thus related to the self-ordering of the vanadium pentoxide within the nano-urchin structure.

Relating the highest frequency observed in the spectra to the vanadium-oxygen bond length in the vanadyl group in vanadium-based oxides is possible according to [24]:

$$R = -\ln \frac{\omega/(21349)}{1.9176} \tag{1}$$

where R is the bond length in Å and ω is the frequency in cm^{-1}. Indeed, from the spectral assignments to peaks in the wavenumber region of the xerogel where conformation-specific information is derived, *i.e.* at 966 cm^{-1} and 1001 cm^{-1}, V=O bond lengths of 0.156 nm and 0.155 nm were estimated, respectively. These two peaks are related to the V^{5+} species; specifically with its $\gamma-$ conformation [23]. The signal at 974 cm^{-1} is due to the distorted conformation of the xerogel chain. These observations are in good agreement with previous reports [21], where the nanostructures exhibit a mixed valence and a distorted lamellar structure. In the case of the nano-urchin, two peaks are observed at 996 cm^{-1} and 1014 cm^{-1} that correspond to the stretching modes of the V=O vanadyl group. Applying the empirical equation from above, the estimated values for the bond lengths in the vanadyl group of the nano-urchin structured vanadium pentoxide are 0.154 nm (V^{5+}) and 0.158 nm ($\gamma-V^{5+}$) respectively. The observation of both signals (see inset to Fig. 4b) with similar intensities infers that the nano-urchin contains divalent vanadium as V^{5+}/V^{4+}. Furthermore, since the V^{4+}=O bond is typically a medium intensity band by comparison to the pentavalent V=O bond [25, 26], our observations suggest that the vanadium in this nanostructure is present as a mixed V^{5+}/V^{4+} valence. Details on the vanadium conformation for all nanostructures examined in this work are outlined in Table 1. Clarification of these findings is presented in the complimentary detailed analysis later in Section III.C.

In the Raman scattering spectra of the nanorods, shown in Fig. 5, signals corresponding to the bending mode of the vanadyl group at 276 and 402 cm^{-1} were observed. Spectral contributions from the stretching vibrational mode of the doubly coordinated oxygen (V_2-O) is also observed at 688 cm^{-1}. In the wavenumber region of the breathing mode (100−150 cm^{-1}) there is a shifted intense band at 135 cm^{-1} corresponding to the V−O stretching mode. It has been previously reported, however, that this band is typically ob-

served at 113 cm^{-1} [12] in the case of the VOx nanotubes. Here, the shift arises from the solid cylindrical structure of the nanorods where the vanadate atomic layers do not roll-up during HT in a similar fashion to that of the nanotubes. The resulting conformation is more ordered, as will be outlined in Section III.C.

To probe the scrolled layers of vanadate within the nanotubes to ascertain as to whether more than one spectral contribution indicative of multiple conformations exists, Raman scattering spectra, shown in Fig. 6, were acquired at different laser power densities. Different varieties of vibrational modes are observed in the spectra. In the wavenumber region 100−550 cm^{-1} (phonon modes), peaks located at 139, 191, 280, and 403 cm^{-1} were observed and are in good agreement with observations from similar systems [21]. The VOx nanotubes studied in this work thus exhibit a well-ordered structure close to that of the lamellar xerogel.

It can be seen from Fig. 6 that the increment in the laser power density improves the signal resolution of the vibrational modes of the nanotubes, in particular that of the vanadyl group. The estimated values of the respective bond lengths indicate that in the nanotubes, the V^{5+} species is predominant and the structure is intermediate between that of the xerogel and the nanotubes reported in Refs [21, 27]. Overall, the increase in laser power density only improves the signal intensities of the weaker vibrational signals. Although an increase in the power does not necessarily imply proportionately deeper penetration, signals arising from deeper in the nanotube toward the core (earlier scrolled layers) do contribute to scattering somewhat. Thus the ordered conformation of the vanadate layers is confirmed at least in the outer scrolls.

A comparison of the vibrational characteristics of the nano-urchin and nanotubes presented here, suggests that the distorted lamellar structure of the vanadate layers forming

the constituent nanotubes of the nano-urchin is less similar to that of the xerogel than stand-alone nanotubes. At wavenumbers greater than 1000 cm^{-1} we observed two distinct peaks at 1371 cm^{-1} and 1590 cm^{-1} in the Raman scattering spectra of the nano-urchin. These signals correspond directly to the surfactant intercalated in the vanadate interlaminar spacings, corroborating the excess of amine in the structure detected by XRD analysis [28–30]. In the case of nanorods, the Raman signal exhibits a medium intensity vibrational band at 987 cm^{-1} arising from the vanadyl group with a corresponding V−O bond length of 0.155 nm indicative of the presence of the $\gamma-V^{5+}$ species. Thus the vanadate conformation dissimilarity between VOx nanotubes and nanorods corroborates the difference observed in the respective position of the V−O stretching mode.

B. Infrared Spectroscopy of Vanadium Pentoxide Nanostructures

Figure 7 shows the infrared absorption spectrum of the vanadium pentoxide xerogel. The xerogel exhibits three different characteristic regions of vibration: the first two, located at 510 cm^{-1} and 742 cm^{-1}, are related to the stretching vibrational mode of the V−O bond. In particular, the symmetric V−O−V stretching mode is that observed at 510 cm^{-1} whereas the signal observed at 742 cm^{-1} represents asymmetric $O-(V)_3$ deformation vibrations of the vanadyl polyhedra [26]. The third band, observed at 1010 cm^{-1}, arises from the stretching vibrational mode of the vanadyl group. We note this to be the vibrational spectrum fingerprint for all nanocomposites studied; these bands and their variations allow direct confirmation determination for each nanostructure. Only the lower frequency vibrations resulting from the organic surfactant used during synthesis show comparable variation. A key observation here is that the xerogel is composed predominantly of vanadium in its neutral pentavalent form, V^{5+}.

For comparison of the organic-inorganic nanostructured lamellar precursors, the spectra are divided in two parts: the spectral contribution from the intercalated organic surfactant and those specific to the inorganic nanostructure. The spectra for the lamellar nanocomposites containing DDA, HDA or ODA, exhibited similar vibrational mode contributions. For example, the overall IR spectrum of the HDA-containing nanocomposite is shown in Fig. 8. The high wavenumber region (>2800 cm^{-1}) is the region of the amine-surfactant spectral contribution. The nano-urchin exhibits characteristic bands at 3135 and 3452 cm^{-1} attributed to the N−H vibrational stretching mode of the HDA surfactant used during the synthesis of the nanocomposite [13, 30]. Intense bands resulting from surfactant molecules are observed at 2917 and 2852 cm^{-1}, related to the axial stretching of aliphatic C−H. Other notable bands are located at 1461 cm^{-1}, related to in-plane symmetric angular deformations of CH_2 species, as well as a band at 735 cm^{-1} corresponding to the C−H bending mode of the methylene group in the surfactant. The band at 1610 cm^{-1} is attributed to the N−H bending mode of the surfactant, and the H−O−H bending mode of the water molecule is also observed [13, 14, 21]. The bands at 949 and 999 cm^{-1} correspond to the vibrational V=O stretching mode (vanadyl oxygen) in the nano-urchin and are considered to be related to the two equivalent V=O groups reported for V_2O_5 nanorods [25, 31].

The observation of H−O−H vibrational modes in the region 3890−3640 cm^{-1} and a weak signal with a maximum at 1796 cm^{-1} indicates a detectable presence of remnant water molecules within the nano-urchin; a separate observation from that of protonated long-chained amines. This observation is in marked contrast to findings by Chen *et al.* [32] who did not detect the presence of water molecules in their nanotubes, a result normally consistent with nanorods and solid nanofibers of V_2O_5 [30, 31].

In post-HT nanotubular compounds containing HDA, the presence of relatively weak

signal at 1575 cm^{-1} is observed; although not shown for clarity, the nanocomposites containing DDA and ODA exhibit very weak corresponding N−H bending vibration signals at 1536 cm^{-1} and at 1554 cm^{-1} respectively. These differences are due to the different interlaminar distance caused by organic chains of different lengths and/or conformation between vanadate layers [15], discussed in more detail in Section III.C. An ordered arrangement of surfactant molecules between vanadate layers ensures rigidity against bending deformations [33].

C. Vibrational Determination of Vanadate Conformation

Figure 9 shows the infrared vibrational spectra of the nano-urchin, nanotubes and nanorods of vanadium pentoxide, synthesized with the HDA surfactant, but in the lower wavenumber region where nanocomposite conformation-specific information is observed, specifically between 1020 and 900 cm^{-1}. The signals exhibited by the nano-urchin show several vibrational modes. In the wavenumber region below 1000 cm^{-1}, specifically in the region of the vanadyl group modes, we observe three distinct bands at 997, 954 and 944 cm^{-1}. In the case of the nanorods, also in the spectral region corresponding to the vanadyl group vibrational modes, characteristic vibrational signals at 998, 983, 957, 936 and 921 cm^{-1} were also observed. By employing Eqn. 1 and Ref. [26], the vibrational signals of the nano-urchin are found to exhibit the presence of the V^{5+} species represented by the spectral bands at 997 and 954 cm^{-1}, seen in Fig. 9 to be predominant. The signal at 944 cm^{-1} corresponds to the $\gamma-V_2O_5$ conformation [26]. In the case of the nanorods, the bands at 998, 983 and 957 cm^{-1} correspond to vibrational modes of the V^{5+} species in the vanadyl group. In stark contrast to the nano-urchin and nanotubes, however, the spectrum of the nanorods exhibits a comparatively intense band at 921 cm^{-1} due to the presence of V^{4+} species. The band

at 906 cm^{-1} in the spectrum of the nanotubes is close to that of $\alpha-V^{4+}$ which is considerably less ordered due to a distorted octahedron-shaped vanadyl unit-cell arrangement. The other bands shown in Fig. 9 correspond to contributions from nanocomposite-surfactant interactions and have not yet been accurately assigned.

The fundamental reason for the differences in vanadate conformation and associated ordering of unit cells can be related to atomic-scale chemistry, or more simply, to the ratio V^{4+}/V^{5+} in the oxide walls of the nanostructures [34]. Attempts have previously been made to determine this ratio in VOx nanorolls [33] using X-ray photoelectron spectroscopy (XPS) but no efforts have yet been reported for vibrational spectroscopic determination nor for structures other than those composed of rolled VOx lamina.

Analysis of the FTIR spectra in Fig. 9 shows that the nano-urchin and nanotubes contain primarily V^{5+} in various co-ordinations when analyzed after their formation. However, even from a xerogel precursor comprising hydrated protons between the layers ($V_2O_5{\cdot}0.6H_2O$), the nanorods exhibit signals characteristic of V^{4+} species. The vibrational assignation in the wavenumber region less than 1000 cm^{-1} for the nano-urchin and nanorods [14, 15, 31], indicates the presence of two conformation types of V_2O_5 (see Table 1) namely $\alpha-V_2O_5$ and $\gamma-V_2O_5$. From Fig. 9, the nanorods exhibit four characteristic signals at $\sim$1000 cm^{-1}, indicating a number of vanadate conformations. In particular, two of these (983 and 998 cm^{-1}) correspond to the $\gamma-$ conformation of V_2O_5 [25]. The vibrational mode observed at 921 cm^{-1} corresponds to the reduced quadravalent vanadium species (V^{4+}). The last of these characteristic signals is a vibrational mode related to the distortion of the vanadyl group but further work is required to accurately assign this mode to a vanadium conformation type. This vibration arises from an interaction from divalent vanadium within the scrolled vanadate layers in the nanorods.

The structure of vanadate rolls, for example, is known to be affected by the V^{4+}/V^{5+} ratio [33]. The nanotube walls are composed of vanadium oxo-anions with either a neutral or negative charge. The presence of V^{5+} neutralizes this charge if present; V^{4+} does not. Consequently, the total anion charge on the nanotube walls is a direct function of the V^{4+} content. As the amine surfactant used in this work is the structural template and also cationic, greater quantities of V^{4+} results in greater quantities of surfactant binding as the associated electrostatic interaction is much stronger than dative bonding between neutral V^{5+} sites and amine head groups [34]. The overall result is that the nanocomposite showing contributions from V^{4+} in their IR spectra are more ordered. From Fig. 9, we observe that the nanorods have a total V^{4+}/V^{5+} ratio of 1:1.3 ($\sim$40% V^{4+}) in good agreement with previous reports of other ordered VOx nanostructures [8, 33, 35, 36].

For the nanotubes, we observe an interesting dependence of crystal order on the length and conformation of amine surfactant used during synthesis that has not been previously observed. Fig. 10 shows the IR spectra of nanotubes synthesized with HDA and ODA surfactants. Further details can be found in Table 1. The spectrum of the HDA-containing nanotubes shows a pronounced absorption peak at 906 cm^{-1} ($\alpha-V^{4+}$), whereas no signals from V^{4+}=O bonds are observed in the spectrum of ODA-containing nanotubes. This increase in order results from two contributory factors: the *all-trans* bilayered configuration of the amine between the vanadate atomic layers [14] and the reduced interatomic distance cause by the shorter alkyl chains. The increased van der Waal's interaction [37] reduces the degree of distortion of the vanadate layers. Thus the associated reduction in the ratio of V^{5+} to V^{4+} allows the nanostructures to form with lower curvature during HT by increasing the inorganic charge density [38] and more effective binding uptake of the amine surfactant between the vanadate layers during synthesis.

Further evidence of the variation in interatomic layer binding and arrangement of the HDA and ODA surfactant in the nanotubes can be seen in Fig. 10, where the shaded area highlights the wavenumber region characteristic of C−H bending vibrations within the methylene group. The difference in the normalized intensities for both curves at ∼735 cm^{-1} relates directly to the quantity of C−H bending vibrations in the methyl group of the surfactant. Since these groups are located along the alkyl chain, significant vibrational contribution to the measured signal can only indicate a greater freedom of movement, or 'wiggle', of the interlayer methylene groups resulting from a less-ordered packing of ODA. This less-ordered packing arrangement is due to either a lower quantity of bound amine head groups on the tube wall for reasons outlined above, or from non-equal positioning of methylene groups within the layers as a result of the deformed (V^{5+}−containing) vanadate conformation [34]. The evidence supports the latter since we previously determined [14] that a bilayer of amine chains in the *all-trans* conformation is oriented in opposite directions within the tube walls with a 10−30% overlap between neighboring chains for angles of 0−30° to the normal to the tube wall.

IV. CONCLUSIONS

Both Raman scattering and infrared spectroscopies showed that the structure of nano-urchin, nanotubes and nanorods of vanadium oxide nanocomposite are strongly dependent on the valency of the vanadium, its associated interactions with the organic surfactant template and the packing mechanism and arrangement of the surfactant between vanadate layers. Accurate assignation of the vibrational modes to the V−O co-ordinations has allowed their comparative classification and relation to atomic layer structure.

The vibrational measurements show varying degrees of crystalline order post-HT even

though all nanostructures stem from the same V_2O_5 xerogel precursor. The solid nanorods exhibit the highest degree of crystalline order, but nanotubes are found to have improved levels of vanadate ordering depending on the length of the alkyl chain in the surfactant. Whereas the nanotube-containing nano-urchin contain vanadate layers in the nanotubes that are in a distorted $\gamma-V^{5+}$ conformation, the vibrational infrared spectra of the nanorods, by comparison, show evidence for V^{5+} and V^{4+} species-containing ordered VOx lamina. This result is even more intriguing when it is known that even a nanocrystal with the complex morphology of vanadium pentoxide nanotubes possesses an atomic arrangement very well defined on the nanometer length scale and well described in terms of a unit cell and symmetry.

V. ACKNOWLEDGMENTS

This material is based upon work supported by the Science Foundation Ireland under Grant No. 02/IN.1/172. Support from FONDECyT (Grants 1050344, 1030102, 7050081), the University of Chile, the Universidad Tecnológica Metropolitana and the EC-funded Network of Excellence P*h*OREMOST (FP6/2003/IST/2-511616) are also gratefully acknowledged.

[1] S. Iijima, *Nature* **354**, 56 (1991).

[2] P. M. Ajayan, S. Iijima, *Nature* **358**, 23 (1992).

[3] A. M. Morales, C. M. Lieber, *Science* **279**, 208 (1998).

[4] Z. W. Pan, Z. R. Dai, Z. L. Wang, *Science* **291**, 1947 (2001).

[5] Y. H. Gao, Y. Bando, T. Sato, *Appl. Phys. Lett.* **79**, 4565 (2001).

[6] W. S. Shi, H. Y. Peng, N. Wang, C. P. Li, L. Xu, C. S. Lee, R. Kalish, S. T. Lee, *J. Am. Chem. Soc.* **123**, 11095 (2001).

[7] P. Gomez-Romero, *Adv. Mater.* **13**, 163 (2001).

[8] F. Krumeich, H.-J. Muhr, M. Niederberger, F. Bieri, B. Schnyder, R. Nesper, *J. Am. Chem. Soc.* **121**, 8324 (1999).

[9] M. E. Spahr, P. Bitterli, R. Nesper, M. Müller, F. Krumeich, H.-U. Nissen, *Angew. Chem. Int. Ed.* **37**, 1263 (1998).

[10] H.-J. Muhr, F. Krumeich, U. P. Schönholzer, F. Bieri, M. Niederberger, L. J. Gauckler, R. Nesper, *Adv. Mater.* **12**, 231 (2000).

[11] M. Niederberger, H.-J. Muhr, F. Krumeich, F. Bieri, D. Günther, R. Nesper, *Chem. Mater.* **12**, 1995 (2000).

[12] G. R. Patzke, F. Krumeich, R. Nesper, *Angew. Chem. Int. Ed.* **41**, 2446 (2002).

[13] C. O'Dwyer, D. Navas, V. Lavayen, E. Benavente, M. A. Santa Ana, G. González, S. B. Newcomb, C. M. Sotomayor Torres, *Chem. Mater.* **18**, 3016 (2006).

[14] C. O'Dwyer, V. Lavayen, S. B. Newcomb, E. Benavente, M. A. Santa Ana, G. González, C. M. Sotomayor Torres, *Electrochem. Solid-State Lett.* **10**, A111 (2007).

[15] V. Lavayen, C. O'Dwyer, M. A. Santa Ana, S. B. Newcomb, E. Benavente, G. González, C. M. Sotomayor Torres, *phys. stat. sol. (b)* **243**, 3285 (2006).

[16] J. F. Xu, R. Czerw, S. Webster, D. L. Caroll, J. Ballato, R. Nesper, *Appl. Phys. Lett.* **79**, 1711 (2002).

[17] G. T. Kim, J. Muster, V. Krstic, J. G. Park, Y. W. Park, S. Roth, M. Burghard, *Appl. Phys. Lett.* **76**, 1875 (2000).

[18] M. Ando, K. Kadono, M. Haruta, T. Sakaguchi, M. Miya, *Nature* **374**, 625 (1995).

[19] M. Malta, G. Louarn, N. Errien, R. Torresi, *Electrochem. Commun.* **5**, 1011 (2003).

[20] P. N. Tririkalitis, V. Petkov, M. G. Kanatzidis, *Chem. Mater.* **15**, 3337 (2003).

[21] A. G. Souza Filho, O. P. Pereira, J. G. Santos, J. Mendes Filho, O. L. Alves, *Nano Lett.* **4**, 2099 (2004).

[22] L. Se-Hee, H. C. Cheong, M. J. Seong, P. Liu, C. E. Tracy, A. Mascarenhas, J. R. Pitts, S. K. Deb, *J. Appl. Phys.* **92**, 1893 (2002).

[23] W. Chen, L. Mai, J. Peng, Q. Xu, Q. Zhu, *J. Solid State Chem.* **177**, 377 (2004).

[24] F. D. Hardcastle, I. E. Wachs, *J. Phys. Chem.* **95**, 5031 (1991).

[25] N. Pinna, M. Willinger, K. Weiss, J. Urban, R. Schögl, *Nano Lett.* **3**, 1131 (2003).

[26] X. Liu, C. Taschenr, A. Leonhardt, M. H. Rummeli, T. Pichler, T. Gemming, B. Buchner, M. Knupfer, *Phys. Rev. B* **72**, 115407 (2005).

[27] J. Cao, J. Choi, J. L. Musfeldt, S. Lutta, M. S. Whittingham, *Chem Mater.* **16**, 731 (2004).

[28] V. Lavayen, M. A. Santa Ana, J. Seekamp, C. M. Sotomayor Torres, E. Benavente, G. González, *Mol. Cryst. Cryst. Liq.* **416**, 49 (2004).

[29] V. Lavayen, *Ph. D. Thesis*, Universidad de Chile (2004).

[30] W. Chen, L. Q. Mai, J. F. Peng, Q. Xu, Q. Y. Zhu, *J. Mater. Sci.* **39**, 2625 (2004).

[31] M. Malta, R. Torresi, G. Louarn, N. Errien, *Electrochim. Acta* **50**, 5009 (2005).

[32] X. Chen, X. Sun, Y. Li, *Inorg. Chem.* **41**, 4527 (2002).

[33] D. Sun, C. W. Kwon, G. Baure, J. MacLean, B. Dunn, S. H. Tolbert, *Adv. Funct. Mater.* **14**, 1197 (2004).

[34] V. Petkov, P. Y. Zavalij, S. Lutta, M. S. Whittingham, V. Paranov, S. Shastri, *Phys. Rev. B* **69**, 085410 (2004).

[35] S. Nordlinder, L. Nyholm, T. Gustafsson, K. Edstrom, *Chem. Mater.* **18**, 495 (2006).

[36] S. Nordlinder, A. Augustsson, T. Schmitt, J. Gou, L. C. Duda, J. Nordgren, T. Gustafsson, K. Edstrom, *Chem. Mater.* **15**, 3227 (2003).

[37] A. Monnier, F. Schuth, Q. Huo, D. Kumar, D. Margolese, R. S. Maxwell, G. D. Strucky, M. Krishmnamurty, P. Petroff, *Science* **261**, 1299 (1993).

[38] S. H. Tolbert, C. C. Landry, G. D. Strucky, B. F. Chmelka, P. Norby, J. C. Hanson, *Chem. Mater.* **13**, 2247 (2001).

Figure Captions

Fig. 1

FESEM micrograph of (a) the nano-urchin and (b) nanorods of vanadium oxide. The inset to (a) shows an array of as-synthesized vnadium pentoxide nanotubes.

Fig. 2

High resolution bright field TEM image of fully developed nanotubes acquired at Scherzer defocus. Lattice planes are clearly resolved at the sidewall regions and a single interatomic layer spacing is marked. The hollow center extends to the tip of the nanotube. From diffraction contrast variations, evidence for the scrolling of the laminar V_2O_5 nanocomposite is clearly visible. (*Inset*) Selected area electron diffraction (SAED) pattern highlighting the principle spacing of 2.85 nm at **U**.

Fig. 3

(a) X-ray diffraction pattern of the post-hydrothermal treatment VOx nanotubes. The resulting phase is $V_2O_5(HDA)_{0.83}{\cdot}1.8H_2O$ and characterized by an interlaminar spacing of 2.9 nm. (b) Higher angle XRD pattern with corresponding indexed $\{hk0\}$ reflections.

Fig. 4

Raman scattering spectrum of the (a) V_2O_5 xerogel (b) nanotubes in the vanadium pentoxide nano-urchin acquired with laser power densities of 1312 and 291 μW μm^{-2} respectively. All major V$-$O$-$V vibrational peaks are marked. The inset plot shows a magnified section of the spectra area between 980 and 1020 cm^{-1} represented by the dashed box.

Fig. 5

Raman scattering spectrum of the vanadium pentoxide nanorods acquired at a laser power density of 291 μW μm^{-2}.

Fig. 6

Raman scattering spectra of the vanadium pentoxide nanotubes acquired at two different laser power densities.

Fig. 7

Infrared spectra of the vanadium pentoxide xerogel prior to organic surfactant intercalation.

Fig. 8

FTIR transmittance spectrum, averaged from 300 scans, of the VOx nano-urchin nanocomposite acquired at room temperature between 4000 and 450 cm^{-1}.

Fig. 9

Infrared spectra of the HDA amine intercalated nano-urchin, nanorods and nanotubes of vanadium pentoxide. The (*) signals correspond to the bands of the V_2O_5 xerogel. The shaded area corresponds to the spectral range of the surfactant vibrational modes.

Fig. 10

Infrared spectra of the nanotubes intercalated with (——) octadecylamine and (− − −) hexadecylamine surfactant.

Compound (Surfactant)	ν_{V-O-V} (cm^{-1})	ν_{V-O-V} (cm^{-1})	$\nu_{V=O}$ (cm^{-1})	Valency Conformation
Xerogel V_2O_5	510	742	1010 (0.154 nm)	$\gamma-V^{5+}$
V_2O_5 lamellar (ODA)	505	726	1012 (0.154 nm)	$\gamma-V^{5+}$
			960 (0.157 nm)	V^{5+}
Nanotubes (ODA)	527	726	960 (0.157 nm)	V^{5+}
			1001 (0.155 nm)	V^{5+}
V_2O_5 lamellar (HDA)	518	730	970 (0.150 nm)	V^{5+}
			1002 (0.155 nm)	V^{5+}
Nanotubes (HDA)	518	–	906 (0.160 nm)	$\alpha-V^{4+}$
			938 (0.158 nm)	V^{5+}
Nano-Urchin	529	797	944 (0.158 nm)	V^{5+}
			954 (0.158 nm)	V^{5+}
			997 (0.155 nm)	$\gamma-V^{5+}$
Nanorods	533	–	921 (0.159 nm)	$\alpha-V^{4+}$
			936 (0.159 nm)	$\alpha-V^{4+}$
			998 (0.155 nm)	$\gamma-V^{5+}$
			957 (0.157 nm)	V^{5+}
			983 (0.156 nm)	V^{5+}

TABLE I: Assignation of the vibrational modes in the range 1020−900 cm^{-1} of the vanadium oxide nanocomposites and nanostructures.

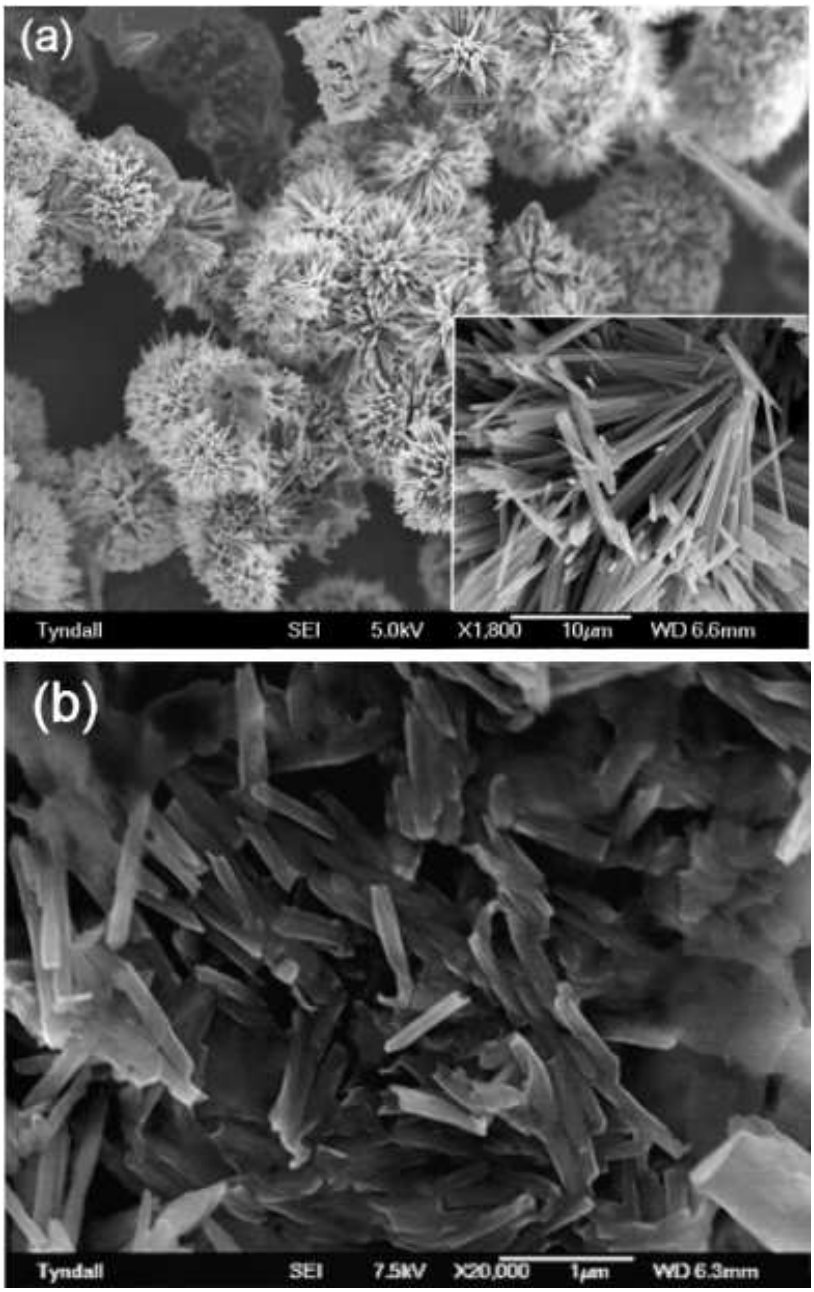
(a)
Tyndall SEI 5.0kV X1,800 10μm WD 6.6mm
(b)
Tyndall SEI 7.5kV X20,000 1μm WD 6.3mm

Fig. 1

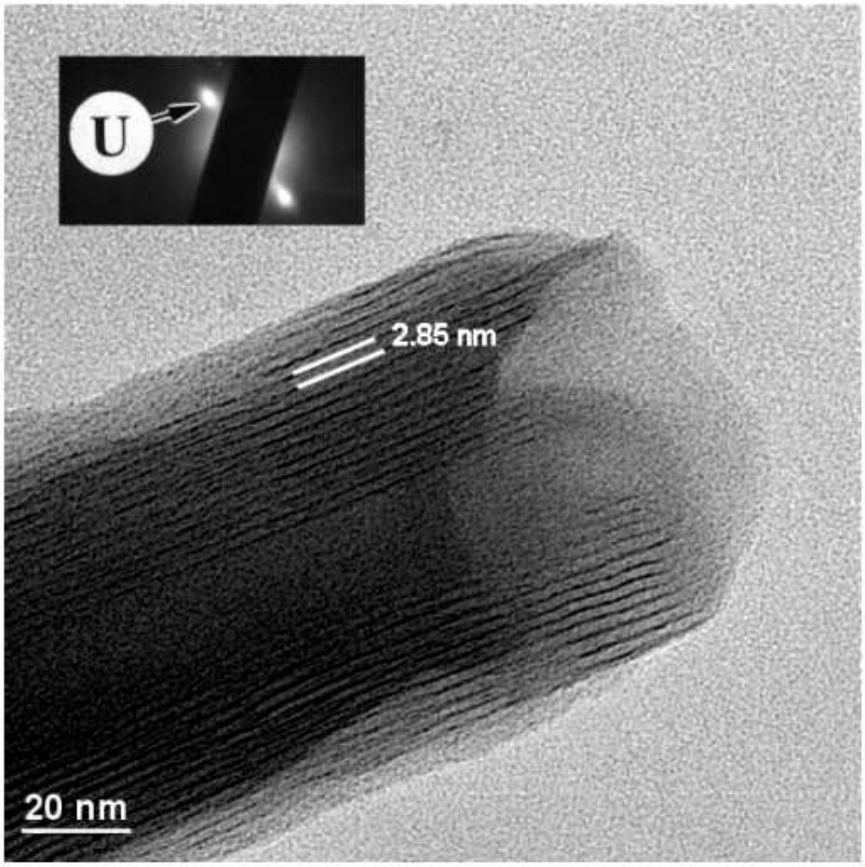

Fig. 2

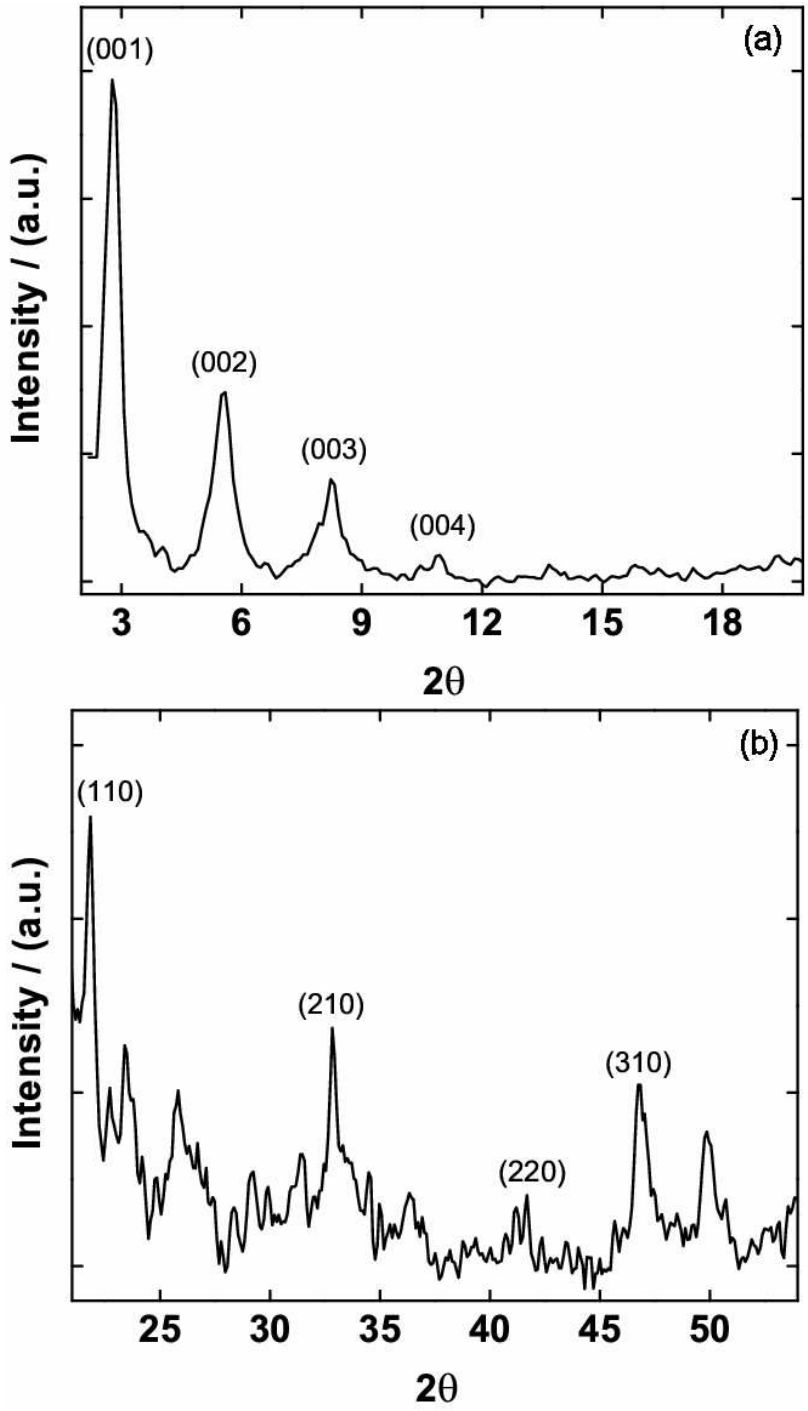
(a)
(001)
(002)
(003)
(004)
Intensity / (a.u.)
3
6
9
12
15
18
2θ
(b)
(110)
(210)
(220)
(310)
Intensity / (a.u.)
25
30
35
40
45
50
2θ

Fig. 3

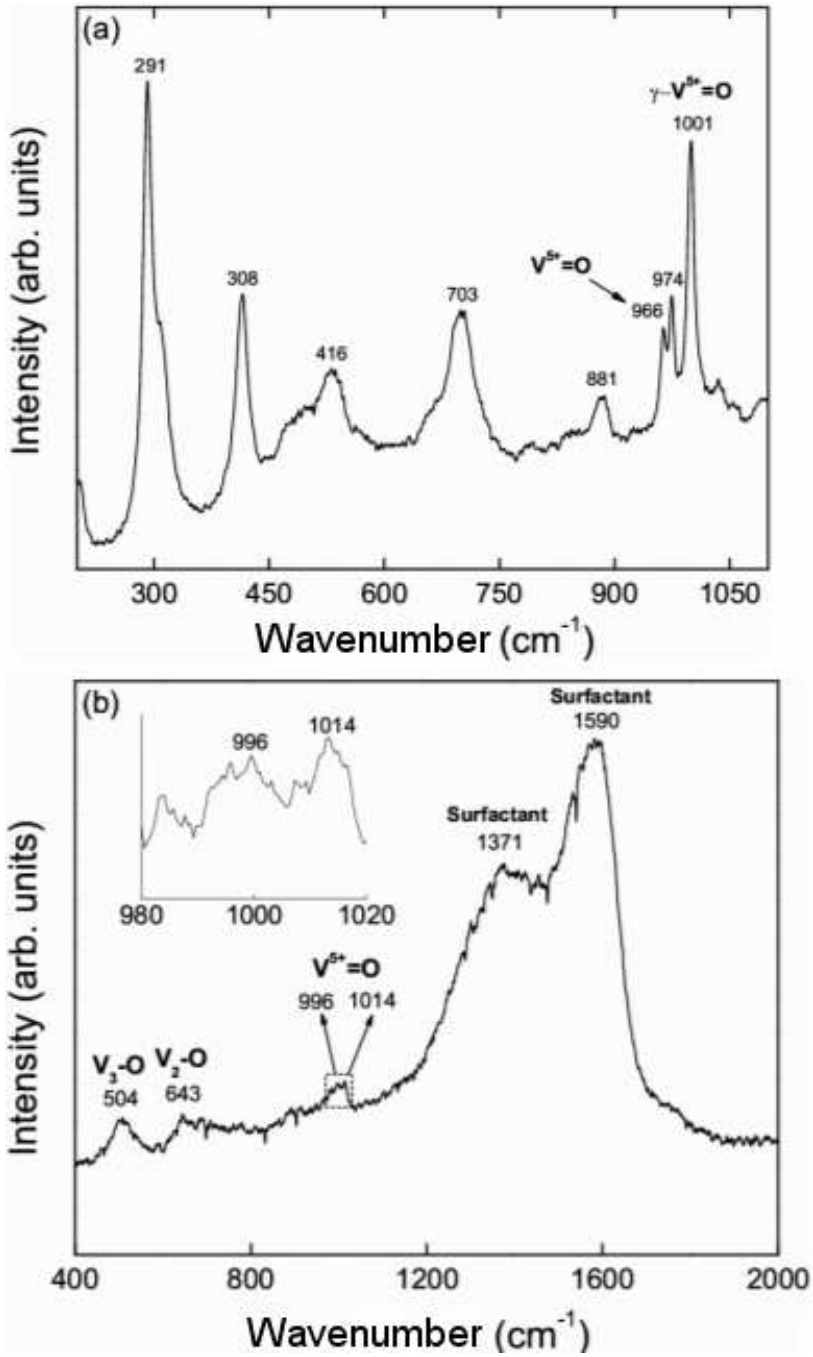
(a)
291
308
416
703
881
966
974
1001
γ-V5+=O
V5+=O
Intensity (arb. units)
300
450
600
750
900
1050
Wavenumber (cm-1)
(b)
996
1014
980
1000
1020
Surfactant
1590
Surfactant
1371
V5+=O
996
1014
V3-O
504
V2-O
643
Intensity (arb. units)
400
800
1200
1600
2000
Wavenumber (cm-1)

Fig. 4

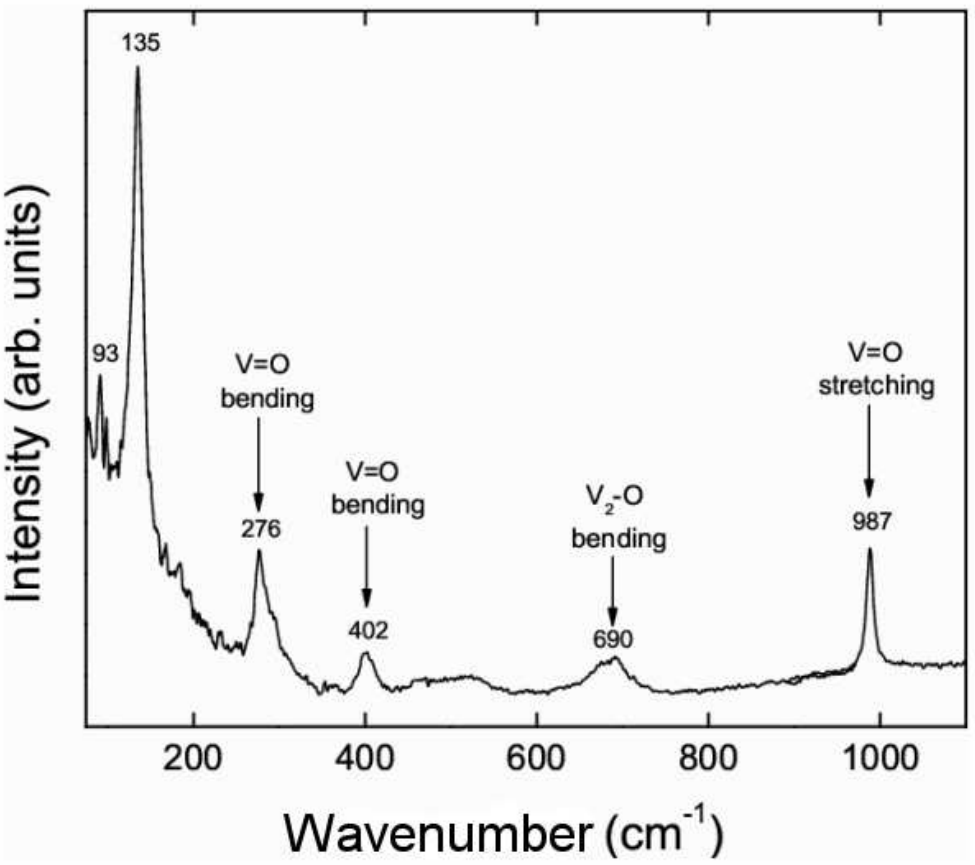
135
93
V=O
bending
276
V=O
bending
402
V2-O
bending
690
V=O
stretching
987
Intensity (arb. units)
200
400
600
800
1000
Wavenumber (cm-1)

Fig. 5

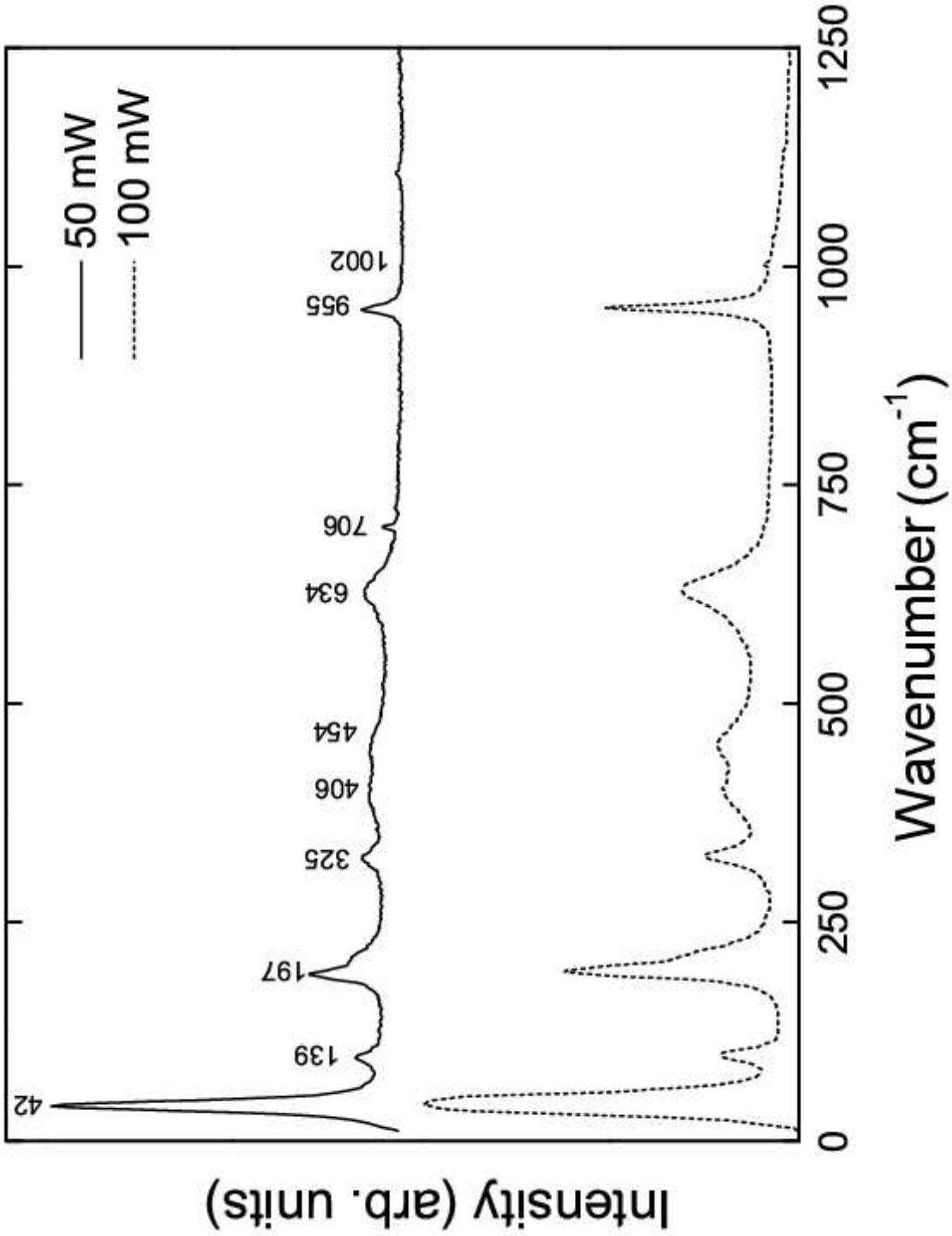
50 mW
100 mW
42
139
197
325
406
454
634
706
955
1002
0
250
500
750
1000
1250
Wavenumber (cm-1)
Intensity (arb. units)

Fig. 6

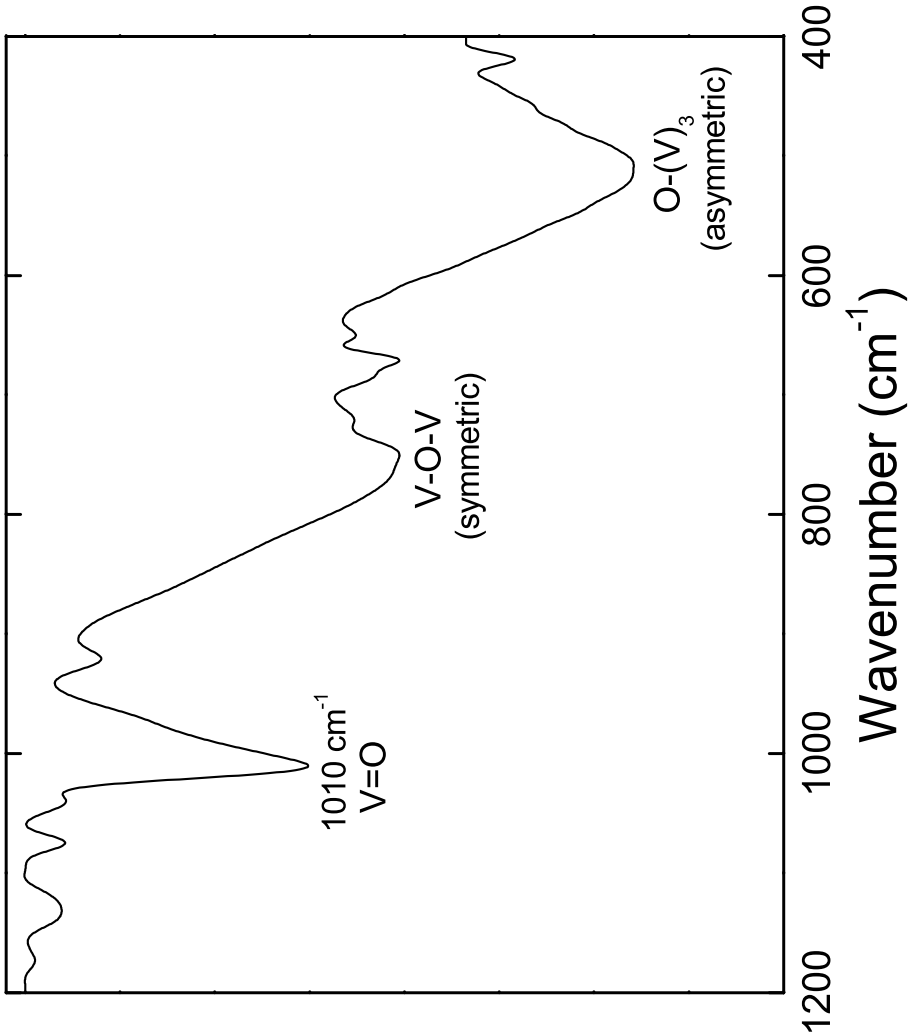
1010 cm-1
V=O
V-O-V
(symmetric)
O-(V)3
(asymmetric)
1200
1000
800
600
400
Wavenumber (cm-1)

Fig. 7

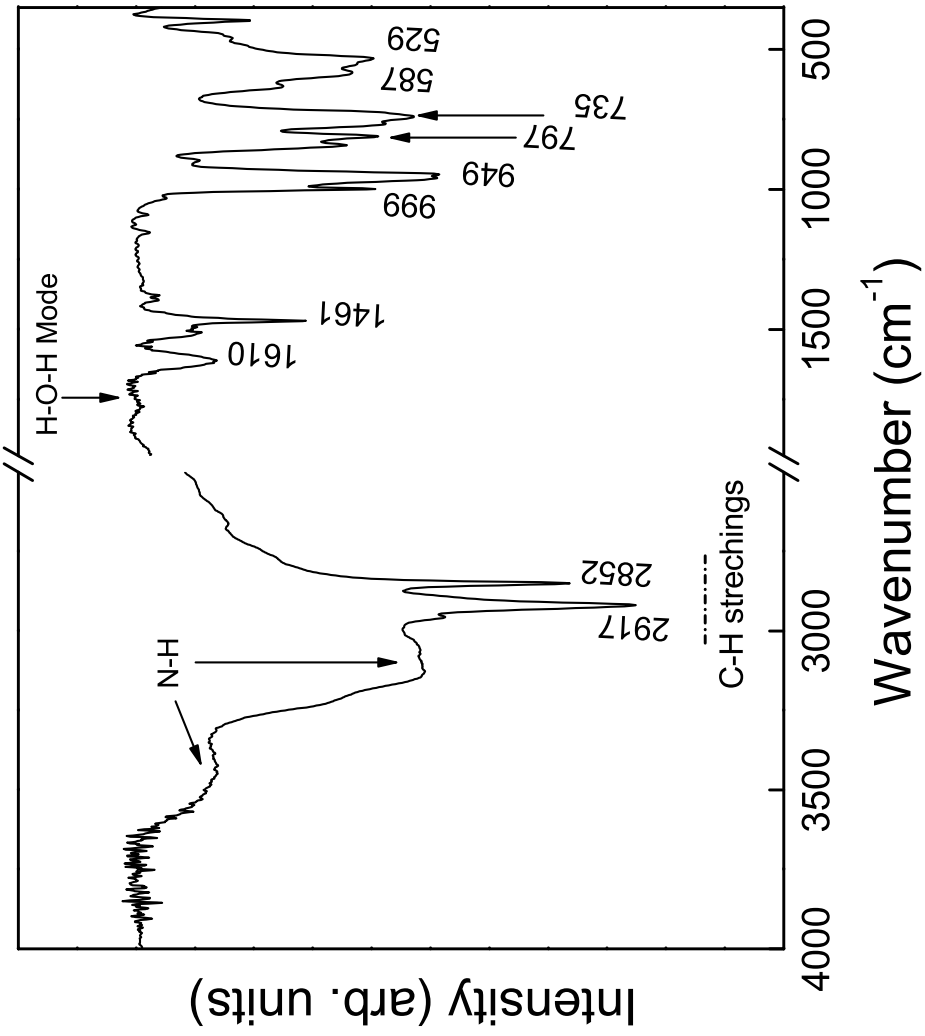
Intensity (arb. units)
Wavenumber (cm^{-1})
4000
3500
3000
2500
2000
1500
1000
500
H-O-H Mode
N-H
C-H strechings
2917
2852
1610
1461
999
949
797
735
587
529

Fig. 8

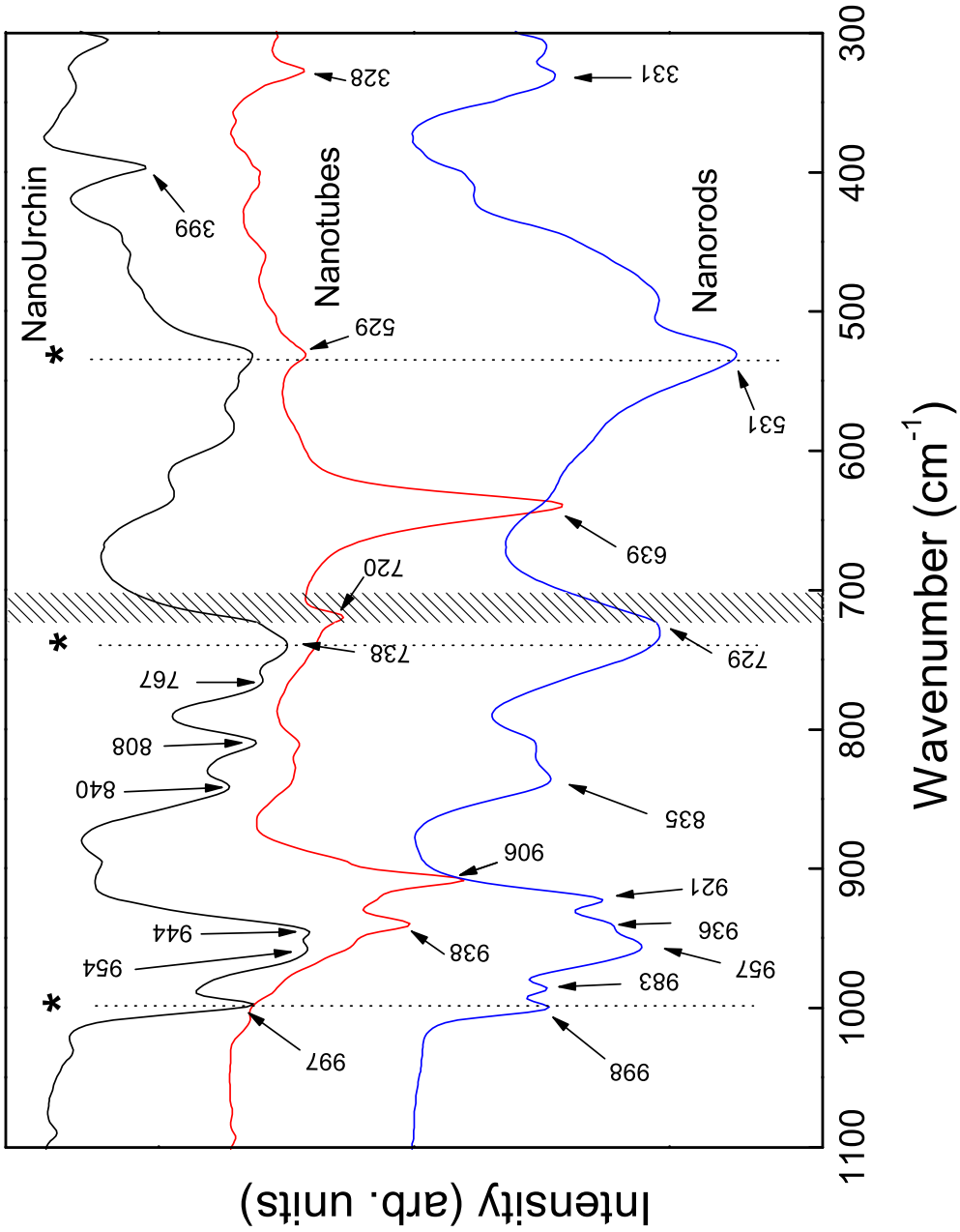
Intensity (arb. units)
Wavenumber (cm-1)
300
400
500
600
700
800
900
1000
1100
NanoUrchin
Nanotubes
Nanorods
399
328
331
529
531
639
720
729
738
767
808
840
835
906
921
936
938
957
944
954
983
997
998
*
*
*

Fig. 9

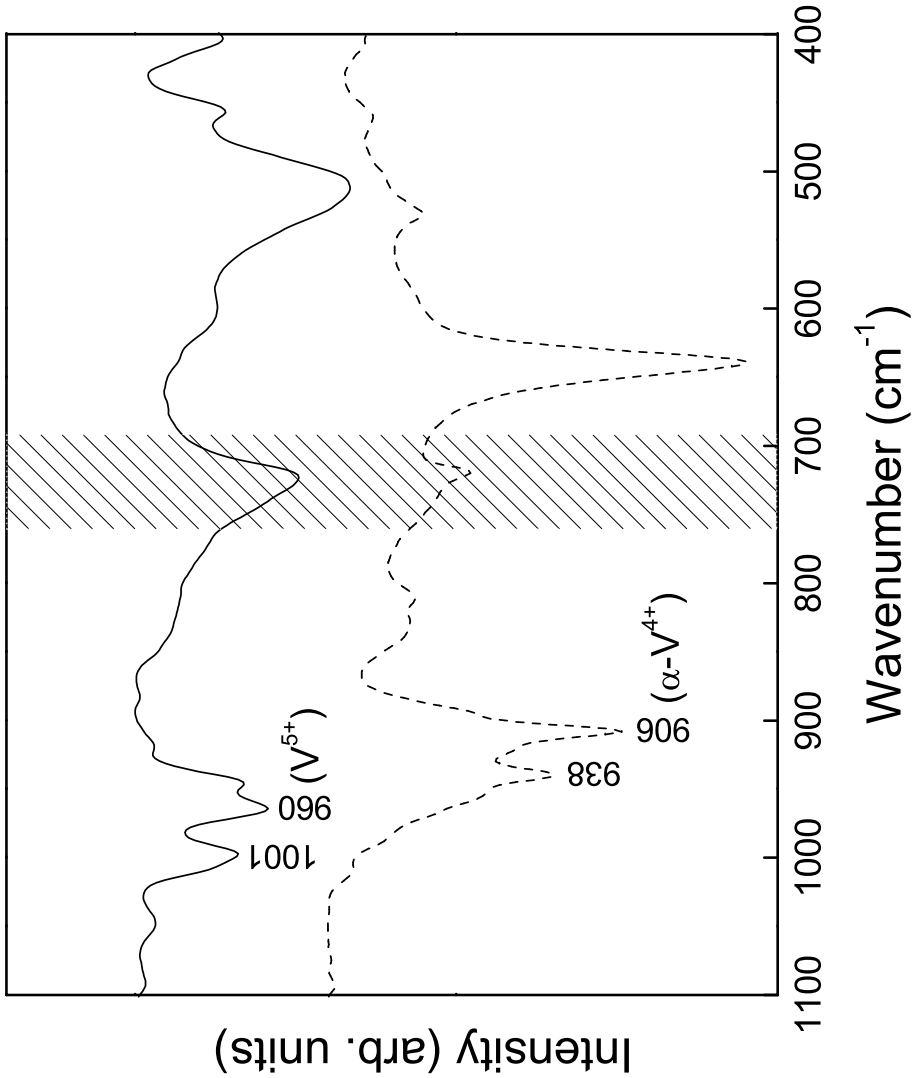
Intensity (arb. units)
Wavenumber (cm-1)
1100
1000
900
800
700
600
500
400
1001
960
(V5+)
938
906
(α-V4+)

Fig. 10